Int J Adv Manuf Technol (2018) 95:1153–1164
https://doi.org/10.1007/s00170-017-1292-z

ORIGINAL ARTICLE

Influence of edge hone radius on cutting forces, surface integrity, and surface oxidation in hard milling of AISI H13 steel

Binxun Li[1,2] · **Song Zhang**[1,2] · **Zhenguo Yan**[1,2] · **Dongdong Jiang**[1,2]

Received: 16 June 2017 / Accepted: 1 November 2017 / Published online: 8 November 2017

Abstract Tool edge preparation has a remarkable influence on tool wear behavior and therefore on the machining performance. In this present research, hard milling of AISI H13 steel (50 ± 1HRC) with uncoated carbide tools was experimentally conducted to identify the effect of an edge hone radius on cutting force, surface integrity (surface roughness, hardness, microstructural changes, and residual stress), and surface oxidation. Experimental results are evaluated by means of an optical profilometer, Nano Tester, optical microscope, SEM, XRD, X-ray stress measurement, and EDS. First, the effect of edge hone radius on cutting forces and surface integrity is significant. That is the cutting and feed forces increase with the increase of edge hone radius, and the lower surface roughness is obtained when using a cutting tool with edge hone radius of 30 μm. Secondly, the nano-hardness in the machined surface, depth of plastic deformation, and compressive residual stress increase with the increase of edge hone radius. Thirdly, neither a white layer nor phase transformation occurs in the machined surface during hard milling process. Finally, no oxygen enrichment and carbon concentration is observed in the subsurface. This research is benefitted to providing a guide to optimize the edge hone radius and acquires a desirable machining performance.

✉ Song Zhang
zhangsong@sdu.edu.cn

[1] School of Mechanical Engineering, Shandong University, 17923 Jingshi Road, Jinan 250061, China

[2] Key Laboratory of High-efficiency and Clean Mechanical Manufacture, Ministry of Education, Shandong University, Jinan, China

Keywords Hard milling · Cutting forces · Nano-indentation · Microstructural changes · Residual stress · Oxidation

1 Introduction

With the advancement of cutting tools and machine tools, hard machining technology has been widely adopted in the fields of manufacturing high-precision automotive and aeronautic components. Milling of hard-to-machine materials into acquired parts has been proved to be a cost-efficient, environment-friendly, and high-throughput method for manufacturing high-quality die and mold components [1–3]. However, tool wear and its sudden fracture exert an adverse effect on cutting force stability and surface integrity. In order to improve the tool life, process stability, and surface integrity, it is possible to realize by better tool edge preparations, such as hone, chamfer, or variable edge radii. Various tool edge geometry has significant influence on cutting force and surface integrity. Surface integrity, including surface roughness, microhardness, microstructural evolution, residual stress, etc., has a direct and remarkable influence on fatigue life of machined components. It can be found that a significant amount of studies on cutting force and surface integrity in hard machining difficult-to-machine materials have been implemented. Cui et al. [4] investigated the high-speed face milling of AISI H13 steel with cubic boron nitride (CBN) tools in a wide range of cutting speed. It was found that a critical speed exists where relatively low mechanical load, long tool life, and cutting force were obtained. Axinte et al. [5] indicated that there were no significant changes in microstructure and microhardness below the machined surface while the lowest surface roughness was acquired within the experimental parameters when high-speed milling H13 steel using coated ball nose end mills. Huang et al. [6] proposed a model to describe the forces due to chip

Table 1 Nominal chemical composition of AISI H13 steel (wt%)

C	Si	Mn	Cr	Mo	V	P	S	Fe
0.32–0.45	0.8–1.25	0.2–0.6	4.75–5.5	1.1–1.75	0.8–1.2	≤ 0.03	≤ 0.03	Balance

Table 2 Thermo-mechanical properties of AISI H13 steel at room temperature

Density (kg/m^3)	Young's modulus (GPa)	Poisson's ratio	Hardness (HRC)	Yield strength (MPa)	Area reduction (%)	Thermal conductivity (W/m·k)	Specific heat (J/kg·k)
7800	211	0.28	50 ± 1	1425	23.0	23.01	417

formation and tool flank wear and compared with experimental data which turns out well matched. Chen [7] suggested that radial force was most sensitive to cutting edge geometry and tool wear when cutting hardened steels with CBN tools. Besides, the finish surface was compatible with the results in grinding process. Sun et al. [8] investigated surface integrity by end milling Ti–6Al–4V. It was concluded that feed rate and depth-of-cut influence surface roughness significantly, and compressive residual stress increases with cutting speed. Additionally, the microhardness on the machined surface is larger than the bulk material. Pu et al. [9] conducted an experimental study to investigate tool wear mechanism and surface integrity with coated tungsten carbide and PCBN tools. PCBN tools produce better surface finish and less work hardening. Du et al. [10] demonstrated the influence of cutting parameters on machined surface plastic deformation and white layer formation through orthogonal milling FGH95 superalloy material. The increasing cutting speed caused severe plastic deformation and a thick white layer. Urbanski et al. [11] conducted high-speed milling of hardened AISI H13 steel experiments to research tool wear, workpiece surface roughness, and cutting force.

However, very little attempts can be found to investigate the effect of edge hone radius on cutting force, surface integrity, and oxidation. Klocke et al. [12] investigated cutting forces and cutting temperature distribution in the tool-chip contact zone for different tool cutting edges. Denkena et al. [13] studied the influence of cutting edge micro-geometry on cutting force and tool wear mechanism in turning operation. Özel et al. [14, 15] found that the cutting edge geometry has significant influence on surface roughness and cutting force. Honed edge geometry resulted in better surface roughness and lower tangential and radial forces. Besides, the advantages of variable edge micro-geometry were presented by comparing the temperature and tool wear distribution. Özel [16] investigated chip morphology, forces, stresses, temperatures, and tool wear through a 3D computational model. Hua et al. [17] indicated that medium edge hone radius (0.02–0.05 mm) plus chamfer is a benefit for keeping temperature and cutting force low, while obtaining a desired residual stress profile. Denkena et al. [18] noted that honed cutting edge enhanced tool life significantly and induced a high tensile residual stress in slot milling of 42CrMo4 Steel. Karpat et al. [19] suggested that edge hone radius must be carefully selected according to specific cutting conditions. The ratio of undeformed chip thickness to edge hone radius around 3 seems to be beneficial for edge preparation. Specifically, due to the variation of undeformed chip thickness in hard milling process, the ratio (r) of undeformed chip thickness (h) to edge hone radius (r_β) usually starts from greater than 1 gradually changing to less than 1, plowing action after shearing plays the dominant role of material removal with honed edge tool which is quite different from milling with a sharp edge tool or turning operation with constant feed rate. As can be seen, among the very little researches in terms of edge hone radius, further insight into the influence of edge hone radius on cutting process, especially for hard face milling process is scant. Consequently, it is of great interest to investigate the effect of edge hone radius for hone tools on cutting forces, surface integrity, and oxidation.

AISI H13 steel as an extremely hard material which combines high temperature strength and excellent wear resistance has been widely used in extrusion, hot forging, and dies and molds casting manufacturing industries. Thus, hard milling

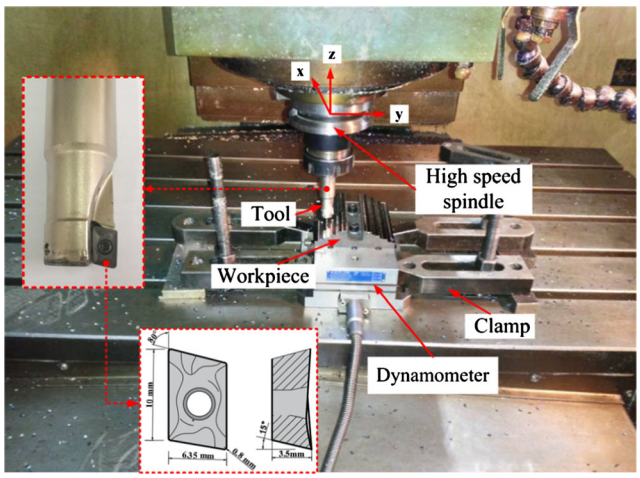

Fig. 1 Description of the experimental workspace

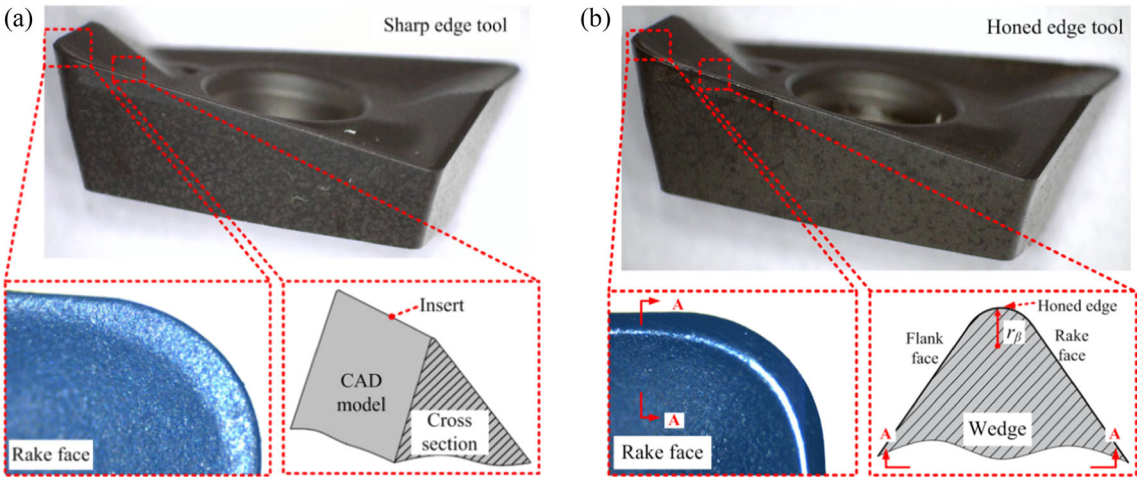

Fig. 2 Characterization of the cutting edge micro-geometry. **a** Sharp edge tool. **b** Honed edge tool

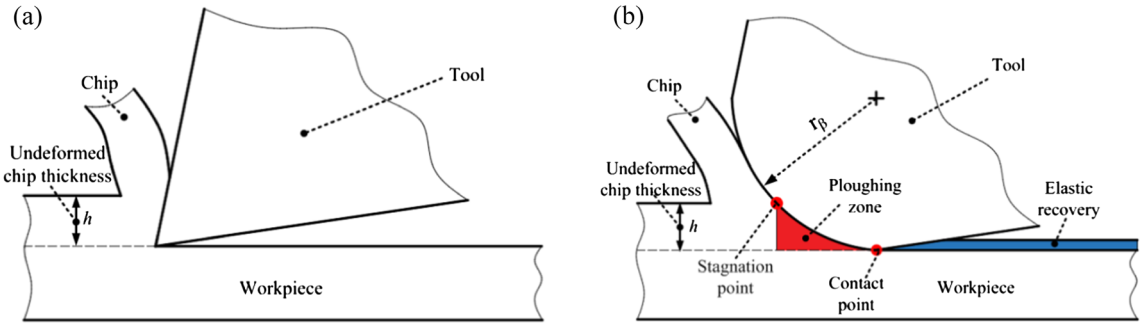

Fig. 3 Characterization of tool contact with machined surface. **a** Sharp edge tool. **b** Honed edge tool

experiments of hardened AISI H13 steel were carried out. The objectives of this research are several folds. First, the effect of edge hone radius on cutting force has been investigated. Secondly, the machined surface integrity including surface roughness, hardness, microstructural changes, and residual stress at different edge hone radii for hone tools are carefully identified and analyzed. Finally, the determination of oxidation reaction on the machined surface is presented.

2 Experimental details

2.1 Workpiece material, machine tool, and cutting tool

In this study, a rectangular block of AISI H13 steel with a dimension of 100 mm × 100 mm × 25 mm which was hardened to 50 ± 1HRC was used in the hard milling experiments. The nominal chemical composition and material mechanical properties of AISI H13 steel are listed in Tables 1 and 2, respectively. The cutting tool employed in hard milling tests was uncoated cemented carbide inserts (XOMX 090308TR-M08, Seco Tools Company, Sweden) mechanically clamped on a tool holder (R217.69-2020.0-09-2A, Seco Tools Company, Sweden) with a diameter of 20 mm which provides an axial rake angle of + 5°, radial rake angle of − 10°, and can be equipped with two inserts. Only one tool insert was applied for each set of milling experiment. Figure 1 shows the experimental setup, milling cutter, and tool insert. All hard milling

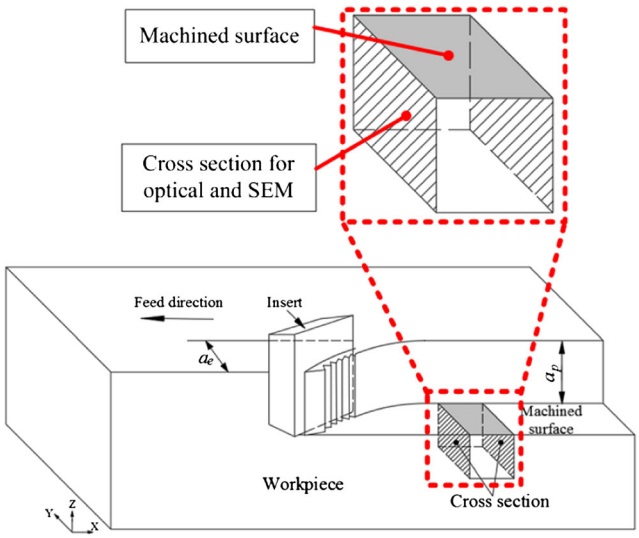

Fig. 4 Sectioning samples preparation for optical and SEM

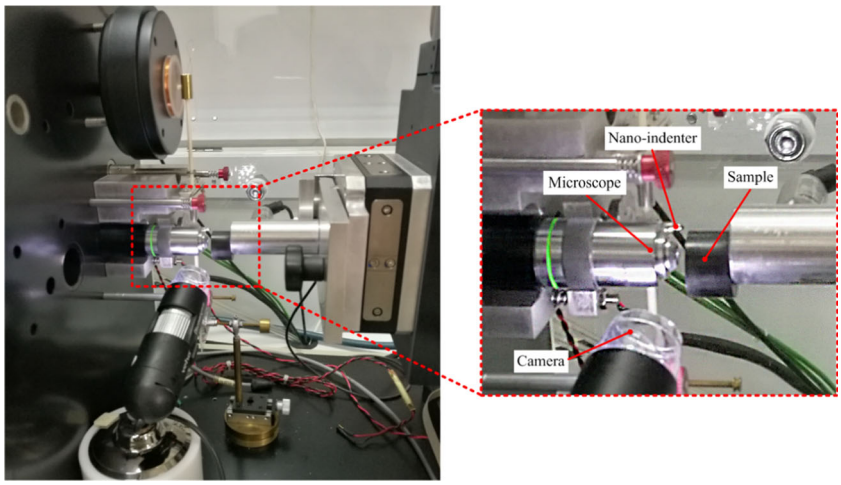

Fig. 5 Nano Tester set up used in experiment

experiments in this research were conducted on a vertical CNC machining center YCM-V116B (YEONG CHIN Company, Taiwan) with an 18.5-KW drive motor and with the maximum spindle rotational speed of 6000 rpm. The cutting edge was honed using brush-honing process by means of a tool edge dulling machine BP-MX (Gerber Company, Switzerland). The Wyko NT9300 (Veeco Company, America) white-light interferometer profiler was employed to measure the edge hone radius r_β [20]. Figures 2 and 3 illustrate the cutting edge geometry preparation and tool-workpiece contact under sharp versus honed edge tool, respectively. As shown in Fig. 3, the contact length is changed between the hone and the workpiece, i.e., the contact length between stagnation point and contact point. Consequently, thermal and mechanical behavior occurred in this area named the plowing zone is bound to influence cutting forces and machined surface integrity.

2.2 Hard milling tests

Down milling was adopted in this research. In order to investigate the effect of edge hone radius on cutting force and machined surface integrity during hard milling AISI H13 steel, the edge hone radius employed in this study was from sharp edge (about 5 μm without pre-treatment) to 120 μm with an incremental step of 30 μm, five sets of experiments in all. The cutting speed, axial and radial depth of cut, and feed rate per tooth were kept constant at 250 m/min, 1.5, 1.5, and 0.2 mm per tooth, respectively. All the milling tests were carried out in dry condition, and each test was replicated three times. The cutting forces in

Table 3 X-ray diffraction parameters for residual stress measurement

X-ray radiation	Bragg angle 2θ	Power	Lattice plane	Exposure time (s)	ψ angles (°)
Cr-Kα	156.4°	30 kV, 6.7 mA	{2 1 1}	25	± 35, ± 25, ± 15, ± 5, 0

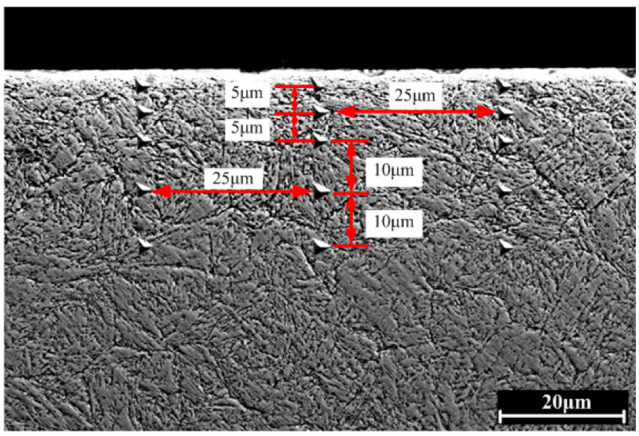

Fig. 6 Indentation of nano-hardness measurement

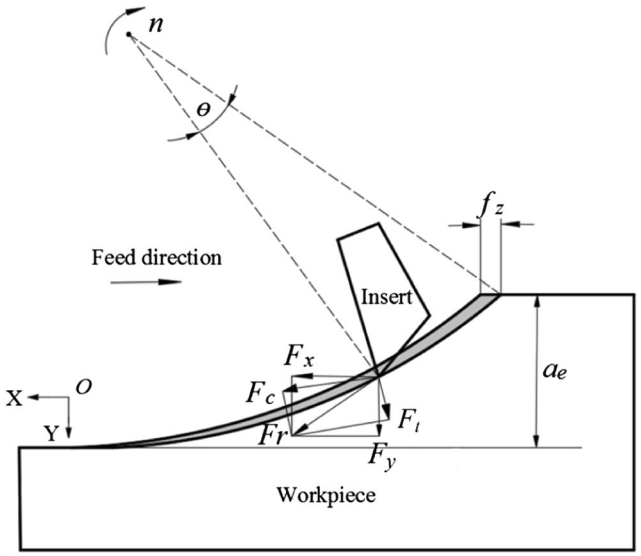

Fig. 7 2D schematic of milling operation

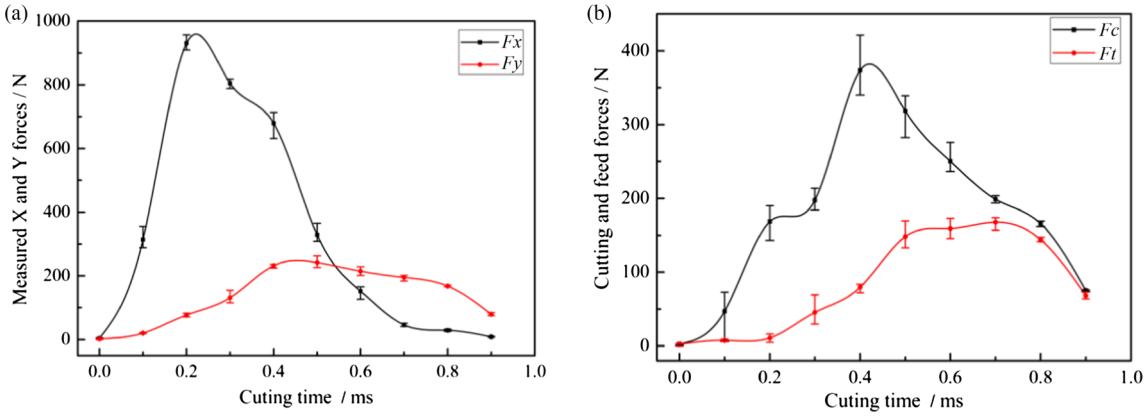

Fig. 8 Forces in 2D hard milling. **a** Measured forces in *X* and *Y* directions. **b** Calculated cutting and feed forces

three directions were measured by means of a Kistler piezoelectric dynamometer (type 9257B, Kistler-Morse Company, Switzerland) which mounted on the machined table as shown in Fig. 1. The charge signal generated at the dynamometer was amplified through multichannel charge amplifiers, acquired and sampled by data acquisition card and Kistler DynoWare software on a personal computer. Measured forces in the *X* and *Y* directions can be resolved into the cutting and feed forces reacting on cutting tool.

2.3 Sample preparation and measurement

To investigate the microstructural evolution below the machined surface as well as the content of chemical elements, workpiece section sample with dimensions of 10 mm × 5 mm × 3 mm was cut out from the machined surface using wire-cut electrical discharge machining (WEDM) after each experiment. The samples were mounted with thermosetting molding compound, polished, and etched in a solution of 5% HNO_3 and 95% ethanol to reveal the microstructure. The cross-section of the samples was examined using an optical microscope (BX41M, Olympus Company, Japan), scanning electron microscope (SEM) (Quanta 250 FEG, FEI Company, America), and energy dispersive spectrum (EDS) (INCA Energy X-MAX-50, Oxford Instruments Company, Britain). Figure 4 shows the section sample for optical, SEM, and EDS. The Wyko NT9300 optical profilometer was adopted to determine the machined surface roughness. The surface roughness values were measured at five equally spaced locations and then averaged the data. Considering the subsurface depth affected by thermal and mechanical load in hard milling process, a Nano Tester was employed in this present work to measure the nano-hardness below the machined surface. The Nano Tester set up is shown in Fig. 5. In terms of the nano-hardness measurements, the penetration of the depth was 500 nm with penetration load 50 mN at the spacing distances of 5 and 10 μm, respectively. For each set of experiments, the nano-hardness measurement was repeated for three times and the average value was acquired so as to eliminate the measurement error. Figure 6 shows the nano-indentation array in the subsurface of workpiece samples. The residual stress in the machined surface has been detected by means of an X-stress

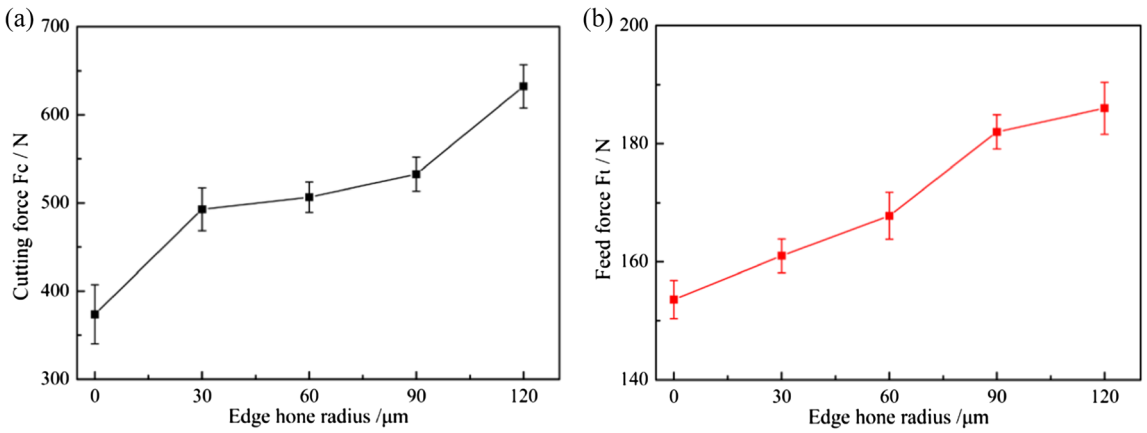

Fig. 9 Effect of edge hone radius on **a** cutting force and **b** feed force

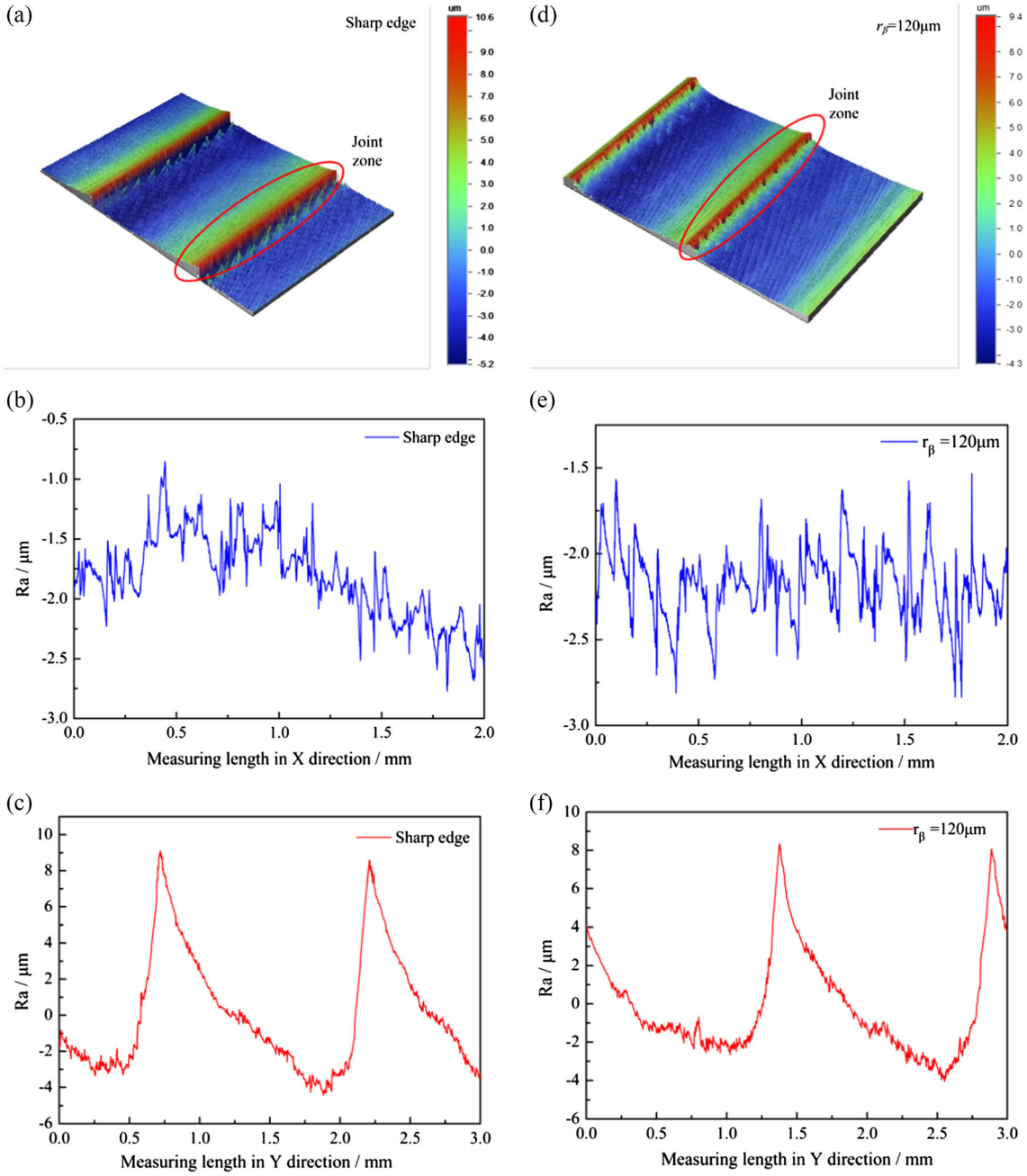

Fig. 10 Surface topography for **a**–**c** sharp edge and **d**–**f** honed edge (r_β = 120 μm). **a** and **d** 3D surface topography. **b** and **e** Surface profile along *X* direction. **c** and **f** Surface profile along *Y* direction

3000 (G2R, Stresstech Oy company, Finland) measurement with $\sin^2\psi$ method [21]. The parameters adopted in the X-ray stress measurement are listed in Table 3.

3 Results and discussion

3.1 Cutting forces

The motion of the insert is the combination of rotation and translation. Thus, the measured forces in the *X* and *Y* directions, F_x and F_y, can be resolved at each cutting tool rotation angle θ in the cutting and feed direction, as shown in Fig. 7. The cutting force F_c and feed force F_t can be obtained using the relations [22]:

$$\begin{cases} F_c = F_x\sin\theta + F_y\cos\theta \\ F_t = F_x\sin\theta - F_y\cos\theta \end{cases} \quad (1)$$

Due to the cutting force is proportional to undeformed chip thickness, hence, the largest cutting force during a milling process appears when the cutting insert just entering the

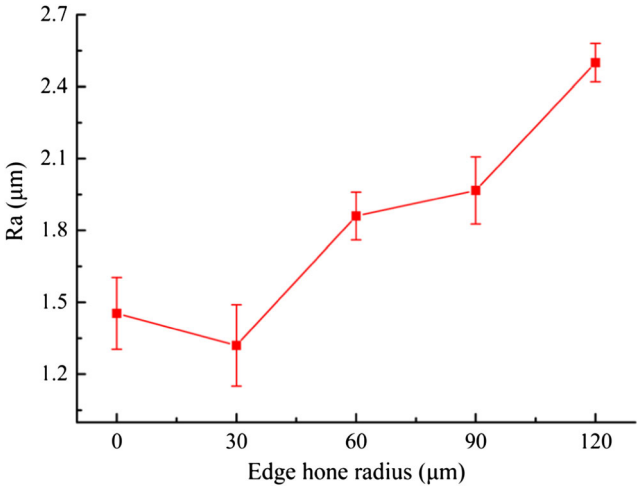

Fig. 11 Effect of edge hone radius on surface roughness

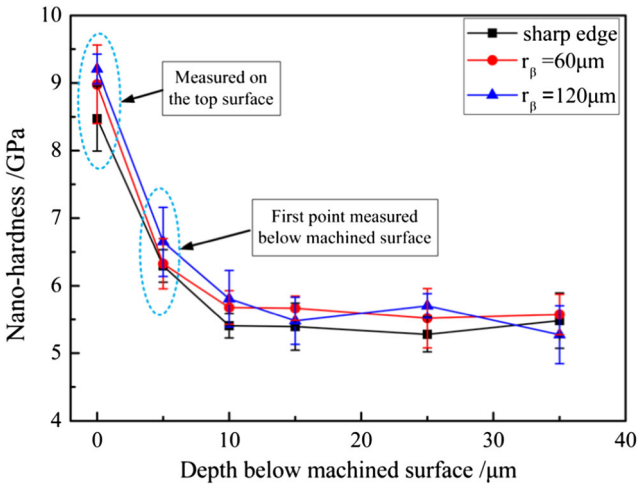

Fig. 12 Nano-hardness distribution below the machined surface

workpiece and the rotation angle θ is very small which can be regarded as zero.

Measured forces in the X and Y directions, F_x and F_y, are shown in Fig. 8a. Forces in the cutting and feed directions, F_c and F_t, are shown in Fig. 8b. As can be seen, the maximum magnitudes of the cutting and feed forces, F_c and F_t, appear when the cutting tool rotates a small angle. It is different from the experimental results in open literature [23]. The possible reason is that the cutting insert does not fully enter the workpiece at the initial stage due to the axial and radial rake angle. With the continued rotation of the cutting tool, the cutting insert is then fully engaged causing high cutting and feed forces. Figure 9 is obtained to illustrate the influence of edge hone radius on cutting and feed forces. The variation of cutting force when edge hone radius ranges from 30 to 90 μm is not pronounced while feed force increases almost linearly with the increase of edge hone radius. This conforms to the experimental results reported in [24]. The evolutions of the cutting and feed forces are possibly attributed to the large contact area between hone and materials ahead of the insert as well as the plowing action. Thus, it has a major influence on the friction between them which conversely results in the higher cutting force. As reported in previous literature [13], higher cutting force resulted from lower edge hone radius which is different from observed in this investigation, whereas the tool wear of the lower edge hone radius tool is much more aggravated than larger edge hone radius tool after removing equal amount of material. That is to say, lower edge hone radius associated with aggravated tool wear in machining process should be responsible for higher cutting force. Conversely, the experimental results in this investigation are in agreement with the reported results. In other words, the cutting tool with large edge hone radius can withstand severe wear and maintain a long tool life due to the changes of characteristic tool wear behavior [18].

3.2 Surface integrity

3.2.1 Surface roughness

As one of the major characteristics to evaluate the machined surface quality, surface roughness is well-connected with tool wear as well as feed rate [25, 26].

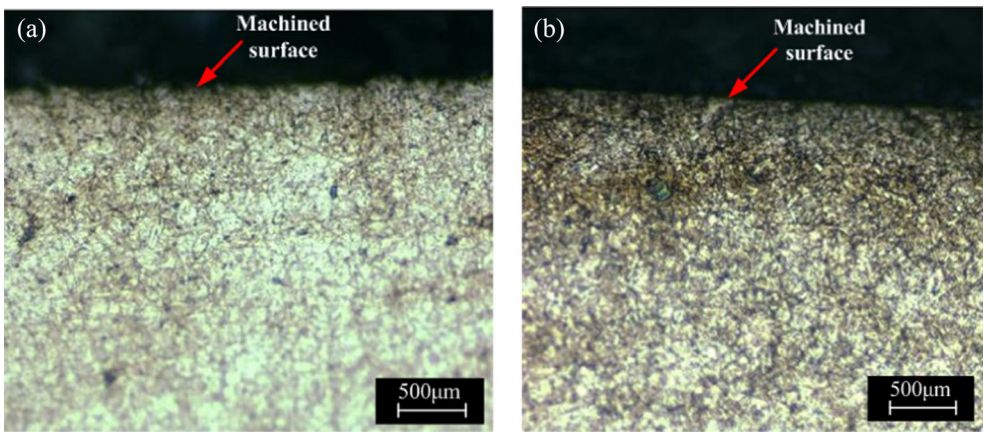

Fig. 13 Optical images of subsurface microstructure. **a** Sharp edge. **b** $r_\beta = 120$ μm

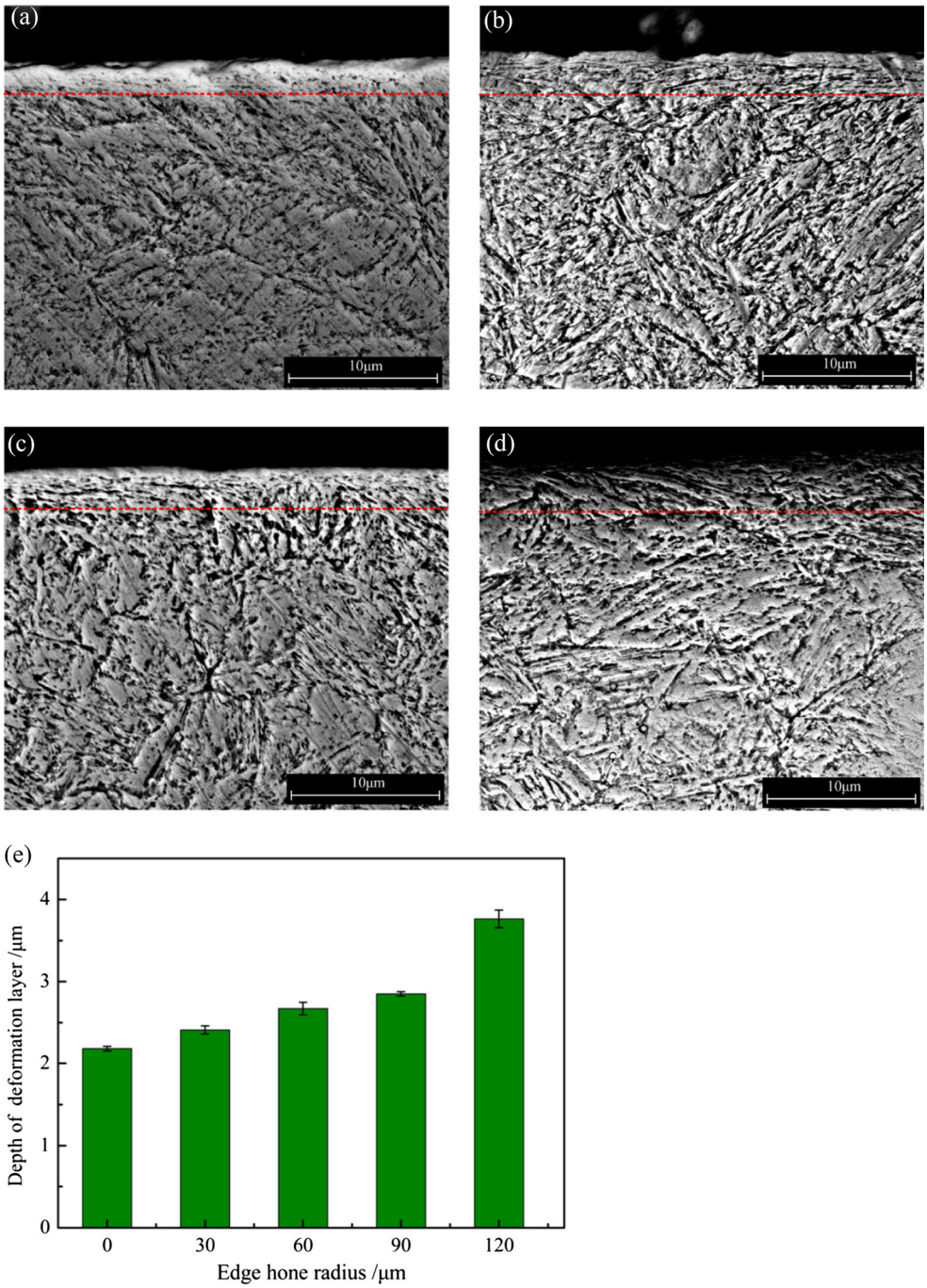

Fig. 14 SEM images of subsurface microstructural. **a** sharp edge. **b** $r_\beta = 60$ μm. **c** $r_\beta = 90$ μm. **d** $r_\beta = 120$ μm. **e** Depth of plastic deformation layer

Arithmetic mean roughness in theory can be estimated as follows [25]:

$$R_a = \frac{f_z^2}{18\sqrt{3}r_e} \tag{2}$$

where f_z is the feed rate and r_e is the nose radius of the cutting tool. As shown in Eq. (2), edge geometry is not involved in empirical and analytical model with respect to surface roughness, whereas edge geometry associated with feed rate plays a major role in determining surface roughness [14, 27]. Figure 10 shows the 3D machined surface topography and its corresponding 2D surface profile. It can be clearly observed that the machined surface appears obvious periodicity in the X direction which is perpendicular to feed direction. The length of a periodicity is equal to the radial depth of cut 1.5 mm. However, periodicity is absent from the milling tests due to the vibration and chatter during machining process in the Y direction, i.e., feed direction. Even though, the tooth marks can be noticed in the 3D surface topography. In contrast with Fig. 10b, the intense fluctuation

of Ra values in Fig. 10e may indicate the change of friction behavior and plowing action. Comparing the acquired surface morphology using sharp and honed edge tool, the joint area generated using honed edge tool shows apparently transitional zone on both sides based on colorbar. Figure 11 is obtained to illustrate the effect of edge hone radius parameter on the machined surface roughness. It is readily apparent that edge hone radius has a significant influence on surface roughness. The surface roughness slightly decreases followed by an increase when the edge hone radius is 30 μm. Specifically, the lowest surface roughness Ra was obtained under the condition of edge hone radius 30 μm. It is in a good agreement with the results in published literature [28]. The deterioration of surface quality under larger edge hone radius is possibly attributed to material side flow caused by flank face due to plowing. Hence, it can be concluded that optimal edge preparation could lead to a better surface roughness.

3.2.2 Surface nano-hardness

Figure 11 demonstrates the distribution of the nano-hardness below the machined surface. It can be observed that the value of nano-hardness on the machined surface is much higher than that in the subsurface, which suggested that work hardening induced by shear plastic strain in hard milling process is responsible for this phenomenon. The first point measured nano-hardness in the subsurface was drastically decreased but still slightly higher than the matrix material (about 5.5 GPa). The experimental results were in close agreement with the previous literature [29] while different from these findings [30, 31]. The differences between these findings are assumed that the size of indenter adopted in Nano Tester is much smaller than Vickers indenter who eliminates the edge effect caused by the indenter size [32]. As shown in Fig. 12, starting from the second point to the last one in the subsurface, the magnitudes of nano-hardness present a relatively stable value which indicates the influence of shear plastic deformation on material is not significant even disappeared. Moreover, it can be concluded that the depth of layer affected by shear plastic deformation is very thin and only about a few microns. This will be further discussed in the following section. Furthermore, it should be pointed out that the nano-hardness of the machined surface increased with the increase of edge hone radius. The possible explanation is that large edge hone radius lead to the increase contact length between tool flank face and machined surface as shown in Fig. 3. Plowing tends to play an important role, and the material becomes intensely compressed.

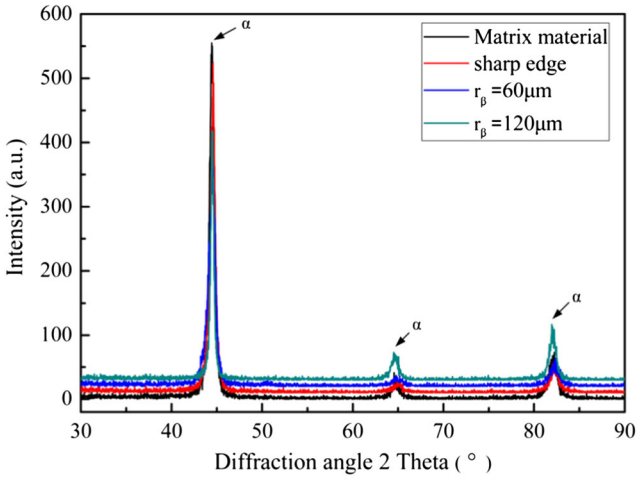

Fig. 15 XRD phase analysis of machined surface

3.2.3 Microstructural changes

Optical and SEM images of the sectioning samples under different edge hone radius are shown in Figs. 13 and 14. As shown in Fig. 13, the white layer was absent from the milling conditions through observing the optical images. Griffiths [33] suggested that the mechanism of white layer formation was attributed to (i) grain refinement induced by plastic deformation, (ii) phase transformation induced by high temperature followed by quickly quenching, and (iii) machined surface reaction with the environment. Severe shear plastic deformation and compact microstructures can be observed in Fig. 14b, c and d while it is not obvious in Fig. 14a. It is likely that the grains are elongated along a certain direction which considered being the opposite feed direction [27]. The thickness of shear plastic deformation layer under different edge hone radius is illustrated in Fig. 14. The thickness of the plastic deformation layer increased from 2.2 to 3.7 μm with the increase of edge hone

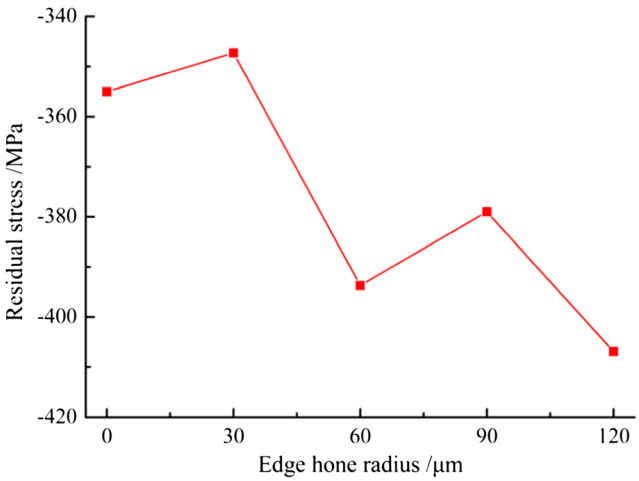

Fig. 16 Measured residual stress on machined surface

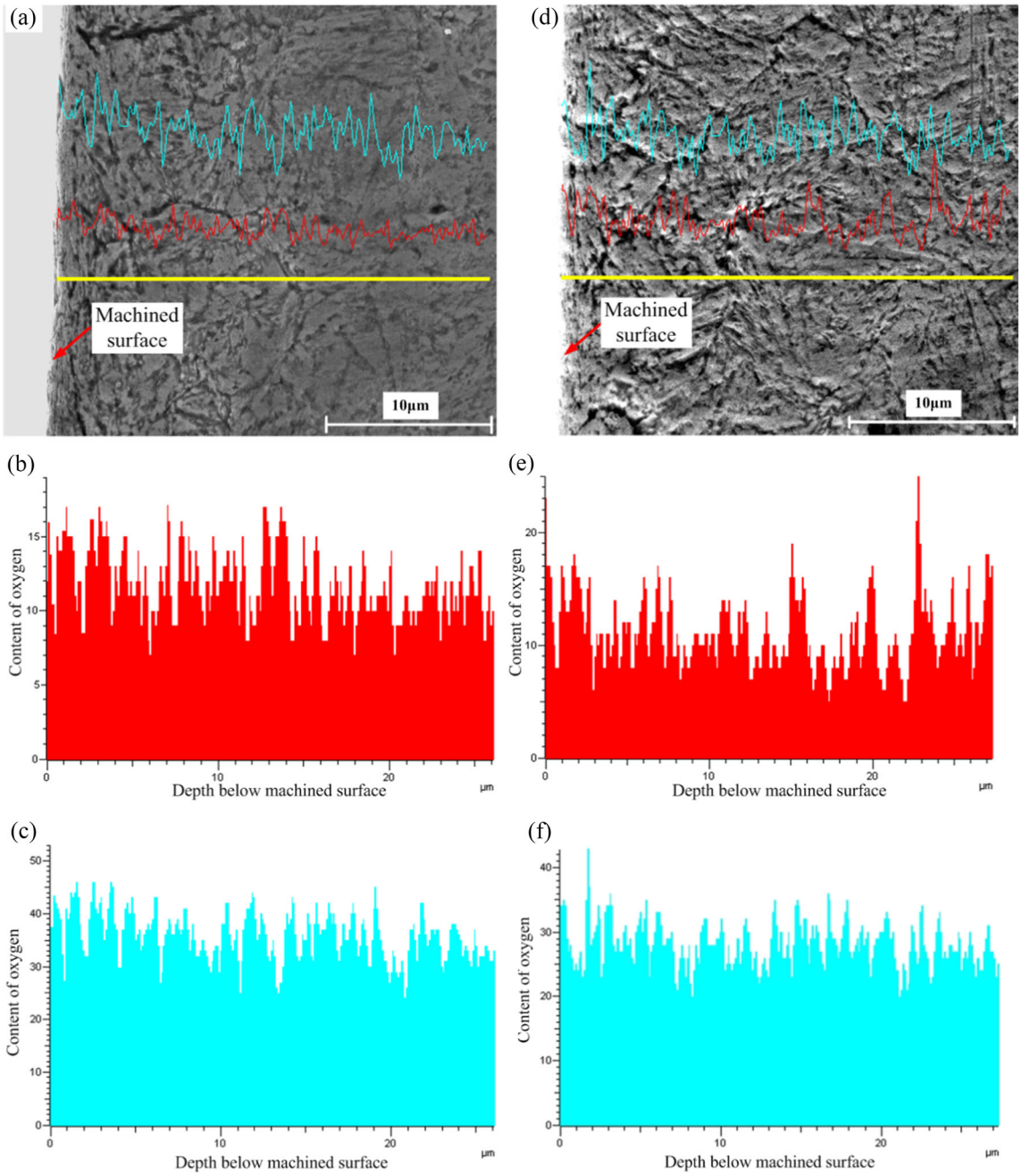

Fig. 17 Relative compositional densities in specimen cross-section for **a**–**c** sharp edge and **d**–**f** honed edge ($r_\beta = 120$ μm). **a** and **d** Sampling location. **b** and **e** Carbon content. **c** and **f** Oxygen content

radius from sharp edge to 120 μm. The possible reason is the high coupling of thermal and mechanical effect induced by severe friction between tool flank face and machined surface as well as shear action and plowing. It is believed that the honed edge often results in the increase of friction, i.e., higher temperature [16].

In order to further verify whether phase transformation occurred in the machined surface or not, an X-ray phase analysis was conducted in this work. Three peaks at 44.44°, 64.66°, and 82.05° can be observed in Fig. 15 based on the phase analysis of matrix material and machined surface under different edge hone radii which referred to ferrite-α according to Bragg's law and data reported in the materials handbook. It can be concluded that no phase transformation occurred in the machined surface despite of the increase of edge hone radius. Consequently, the high nano-hardness presented in the machined surface mentioned above is a result of grain refinement induced by shear plastic strain rather than phase transformation.

3.2.4 Surface residual stress

The flow direction of material can be affected by honed edge tool compared with sharp edge tool and plowing with elastic recovery plays a significant role when edge hone radius is similar or greater than undeformed chip thickness. Figure 16 shows the measured residual stress in the direction which is perpendicular to the feed direction in depth of t_{max} = 5 μm. It can be noted that the residual stress that exists on the machined surface shows compressive stress, and its absolute value increases in fluctuation from 355 to 410 MPa with increases of edge hone radius. This trend is in consistent with a previous report in the literature [33], whereas it is different from the report in the literature [18] that tensile residual stress is generated in the subsurface in slot milling. It is due to the fact that large edges hone radius results in a relatively large plowing area, and more materials in this area become compressed which causes severe plastic deformation in the subsurface. Consequently, it is a result of mechanical load that favors the compressive residual stress.

3.3 Oxidation analysis of machined surface

It has been commonly believed that chip back surface is susceptible to oxidation when exposed to air at higher temperature in hard milling process. The possible oxidation reaction between Fe and O are listed as follows [34]:

$$2Fe(s) + O_2(g) \rightarrow 2FeO(s) \quad (3)$$

$$^{2}/_{3}Fe(s) + O_2(g) \rightarrow {}^{1}/_{2}Fe_3O_4(s) \quad (4)$$

$$^{4}/_{3}Fe(s) + O_2(g) \rightarrow {}^{2}/_{3}Fe_2O_3(s) \quad (5)$$

The oxidation of iron in air proceeded in the following stages [35]:

$$FeO \rightarrow Fe_3O_4 \rightarrow \alpha - Fe_2O_3 \quad (6)$$

As known to all, the colors of FeO, Fe_3O_4, and Fe_2O_3 exhibit blue, dark, and red, respectively. It depends on the degree of oxidation. The colors of chips obtained in this work vary from purple to dark blue with the increase of edge hone radius which suggests the rise of machining temperature. The cutting temperature, exposure time, and surface area, etc. have a significant influence on the occurrence of oxidation reaction. As can be seen from Eqs. (4)–(6), once the oxidation reaction occurs, there is no doubt that the increase of oxygen concentration on the surface inevitably will result in the oxygen enrichment. Considering that the honed tool edge has a major influence on friction between hone and workpiece, thus the temperature correlated with friction and plastic deformation induced by plowing assumed to increase as well. Once the oxidation occurs on the machined surface, the physical and mechanical properties of the material could change as well. Therefore, it is necessary to investigate the oxidation reaction on the machined surface.

EDS analysis was conducted to identify the chemical compositions on the machined surface so as to verify the occurrence of oxidation reaction. The results of EDS analysis are shown in Fig. 17. This figure only shows the effects of sharp edge and edge hone radius 120 μm, because different edge hones in this study lead to similar results. Hence, only the extreme values of tool edge geometry are discussed for clarity. It is noticed that the intensity of oxygen and carbon contents on the machined surface shows no pronounced increase comparing honed edge with sharp edge condition. In addition, even though the honed edge changes the contact and friction behavior as well as temperature distribution, chemical elements content in the subsurface almost keep unvaried in contrast with the matrix material. It can be assumed that the contact length between hone and workpiece causes the reduction of surface area with the environment, or the temperature is not high enough due to quick heat transfer from workpiece to cutting tool which inhibits the occurrence of oxidation. Moreover, the carbon content keeps unvaried in the subsurface further indicates that work hardening induced by severe plastic deformation in the subsurface is the main reason attributed to the higher hardness on the machined surface.

4 Conclusions

In this work, hard milling experiments of hardened AISI H13 steel was conducted to investigate the effects of honed edge tool on cutting force and machined surface integrity. The major conclusions can be summarized as follows:

1. Cutting tool with large edge hone radius results in higher cutting force due to the combination of plowing action and severe friction between hone and materials.
2. As the edge hone radius increased, surface roughness Ra decreased first and then continues to increase. In this study, the lowest surface roughness Ra is obtained under the condition of edge hone radius 30 μm. This outcome may be seen as beneficial for improving surface roughness with proper micro-geometry edge design.
3. The nano-hardness on the machined surface is much higher than that in the subsurface. Since no phase transformation occurs in the machined surface, thermal and mechanical load induced by severe shear plastic deformation would be the predominant mechanism determining the machined surface nano-hardness. Moreover, the nano-hardness and depth of plastic deformation increase with the increase of edge hone radius. White layer is absent from the hard milling conditions. And the content

of oxygen and carbon almost keep unvaried despite of the edge hone radius.

4. The surface residual stress shows compressive residual stress and its absolute value increases with edge hone radius. It is suggested that fatigue microcracks that often occur in a machined surface could be inhibited.

Funding information This work was supported by the National Natural Science Foundation of China (Grants No. 51575321 and No. 51175309) and Taishan Scholars Program of Shandong Province.

References

1. Byrne G, Dornfeld D, Denkena B (2003) Advanced cutting technology. Annals CIRP 52(2):483–507
2. Dewes RC, Aspinwall DK (1997) A review of ultra-high speed milling of hardened steels. J Mater Process Technol 69:1–17
3. Aspinwal DK, Dewes RC (1994) EPSRC case for support-ultra high speed machining of hardened ferrous alloys. School of Mechanical Engineering, University of Birmingham, Birmingham
4. Cui X, Zhao J, Tian X (2013) Cutting forces, chip formation, and tool wear in high-speed face milling of AISI H13 steel with CBN tools. Int J Adv Manuf Technol 64(9):1737–1749
5. Axinte DA, Dewes RC (2002) Surface integrity of hot work tool steel after high speed milling-experimental data and empirical models. J Mater Process Technol 127(3):325–335
6. Huang Y, Liang SY (2005) Modeling of cutting forces under hard turning conditions considering tool wear effect. J Manuf Sci Eng. Trans ASME 127(2):262–270
7. Chen W (2000) Cutting forces and surface finish when machining medium hardness steel using CBN tools. Int J Mach Tools Manuf 40:455–466
8. Sun J, Guo YB (2009) A comprehensive experimental study on surface integrity by end milling Ti–6Al–4V. J Mater Process Technol 209(8):4036–4042
9. Pu Z, Singh A (2013) High speed ball nose end milling of hardened AISI A2 tool steel with PCBN and coated carbide tools. J Manuf Process 15(4):467–473
10. Du J, Liu ZQ (2013) Influence of cutting speed on surface plastic deformation and white layer formation of FGH95. Key Eng Mater 589-590:70–75
11. Urbanski JP, Koshy P, Dewes RC, Aspinwall DK (2000) High speed machining of moulds and dies for net shape manufacture. Mater Des 21(4):395–402
12. Klocke F, Kratz H (2005) Advanced tool edge geometry for high precision hard turning. Annals CIRP 54(1):47–50
13. Denkena B, Becker JC, de Leon-Garcia L (2005) Study of the influence of the cutting edge microgeometry on the cutting forces and wear behavior in turning operations. In: Proceedings of the 8th CIRP. International Workshop on Modelling of Machining Operations, Chemnitz, pp 503–507
14. Özel T, Hsu TK, Zeren E (2005) Effects of cutting edge geometry, workpiece hardness, feed rate and cutting speed on surface roughness and forces in finish turning of hardened AISI H13 steel. Int J Adv Manuf Technol 25(3):262–269
15. Özel T, Karpat Y, Srivastava AK (2008) Hard turning with variable micro-geometry PcBN tools. CIRP Annals—Manuf Technol 57: 73–76
16. Özel T (2009) Computational modelling of 3D turning: influence of edge micro-geometry on forces, stresses, friction and tool wear in PcBN tooling. J Mater Process Technol 209(11):5167–5177
17. Hua J, Shivpuri R, Cheng XM, Bedekar V, Matsumoto Y, Hashimoto F, Watkins TR (2005) Effect of feed rate, workpiece hardness and cutting edge on subsurface residual stress in hard turning of bearing steel using chamfer and hone edge geometry. Mater Sci Eng A 394:238–248
18. Denkena B, Koehler J, Rehe M (2012) Influence of the honed cutting edge on tool wear and surface integrity in slot milling of 42CrMo4 steel. Procedia CIRP 1(1):190–195
19. Karpat Y, Özel T (2008) Mechanics of high speed cutting with curvilinear edge tools. Int J Mach Tools Manuf 48(2):195–208
20. Schimmel RJ, Manjunathaiah J, Endres WJ (2000) Edge radius variability and force measurement considerations. J Manuf Sci Eng 122:590–593
21. Noyan IC, Cohen JB (1987) Residual stress-measurement by diffraction and interpretation. Springer, New York
22. Young HT, Mathew P, Oxley PLB (1994) Predicting cutting forces in face milling. Int J Mach Tools Manuf 34(6):771–783
23. Shatla M, Kerk C, Altan T (2001) Process modeling in machining. Part I: determination of flow stress data. Int J Mach Tools Manuf 41(10):1511–1534
24. Ventura CEH, Chaves HS, Rubio JCC, Abrão M, Denkena B, Breidenstein B (2016) The influence of the cutting tool microgeometry on the machinability of hardened AISI 4140 steel. Int J Adv Manuf Technol 90:2557–2565
25. More AS, Jiang W, Brown WD, Malshe AP (2006) Tool wear and machining performance of cBN–TiN coated carbide inserts and PCBN compact inserts in turning AISI 4340 hardened steel. J Mater Process Technol 180:253–262
26. Oliveira AJ, Diniz AE, Ursolino DJ (2009) Hard turning in continuous and interrupted cut with PCBN and whisker-reinforced cutting tools. J Mater Process Technol 209(12–13):5262–5270
27. Thiele JD, Melkote SN (1999) Effect of cutting edge geometry and workpiece hardness on surface generation in the finish hard turning of AISI 52100 steel. J Mater Process Technol 94:216–226
28. Zhao T, Zhou JM, Bushlya V, Ståhl JE (2017) Effect of cutting edge radius on surface roughness and tool wear in hard turning of AISI 52100 steel. Int J Adv Manuf Technol 91:1–8
29. Wang FZ, Zhao J, Li A, Zhang H (2014) Effects of cutting conditions on microhardness and microstructure in high-speed milling of H13 tool steel. Int J Adv Manuf Technol 73(1):137–146
30. Li W, Guo YB, Guo CS (2013) Superior surface integrity by sustainable dry milling and impact on fatigue. CIRP Ann Manuf Technol 62(1):567–570
31. Zhang S, Ding TC, Li JF (2012) Microstructural alteration and microhardness at near-surface of AISI H13 steel by milling. Mach Sci Technol 16:473–486
32. Hashimoto F, Guo YB, Warren AW (2006) Surface integrity difference between hard turned and ground surfaces and its impact on fatigue life. CIRP Ann Manuf Technol 55(1):81–84
33. Griffiths BJ (1985) White layer formations at machined surfaces and their relationship to white layer formations at worn surfaces. J Tribol 107(2):165–171
34. Zhang S, Guo YB (2009) An experimental and analytical analysis on chip morphology, phase transformation, oxidation, and their relationships in finish hard milling. Int J Mach Tools Manuf 49(11):805–813
35. Chen RY, Yeun WYD (2003) Review of the high-temperature oxidation of iron and carbon steels in air or oxygen. Oxid Met 59(5): 433–468